Supporting Information

3D defect-enriched Cu/Cu$_2$O-Al$_2$O$_3$ zigzag nanostructure for efficient degradation of tetracycline antibiotics

Dandan Wu[a],*, Jicheng Wu[a], Lin Fu[b], Runping Jia[a],*, Qingsheng Wu[b], Yuanzheng Zhu[c], Sheng Han[d], Ming Wen[b],*

[a.]School of Materials Science and Engineering, Shanghai Institute of Technology, 100 Haiquan Road, Shanghai 201418, R. P. China.

[b.]School of Chemical Science and Engineering, Shanghai Key Laboratory of Chemical Assessment and Sustainability, Tongji University, 1239 Siping Road, Shanghai 200092, R. P. China.

[c.]School of Materials and Chemistry, University of Shanghai for Science and Technology, 516 Jungong Road, Shanghai, 200093, P. R. China

[d.]School of Chemical and Environmental Engineering, Shanghai Institute of Technology, 100 Haiquan Road, Shanghai 201418, R. P. China.

Corresponding Authors

* Dandan Wu: wdan1008@163.com, Runping Jia: jiarp@sit.edu.cn, Ming Wen: m_wen@tongji.edu.cn;

1. Experimental Supplement

1.1. Chemicals

Copper nitrate trihydrate ($Cu(NO_3)_2 \cdot 3H_2O$, ≥99.0%), ferric nitrate nonahydrate ($Fe(NO_3)_3 \cdot 9H_2O$, ≥99.99%), aluminum nitrate nonahydrate ($Al(NO_3)_3 \cdot 9H_2O$, ≥ 99.0%), urea (H_2NCONH_2, AR), absolute ethanol (CH_3CH_2OH, ≥99.7%), triethanolamine (TEA, $C_6H_{15}NO_3$, AR), tert-butanol (TBA, $C_4H_{10}O$, AR), p-benzoquinone (BQ, $C_6H_4O_2$, ≥97.0%), . All the above reagents were provided by Shanghai Aladdin Reagent Co., Ltd. Sodium hydroxide (NaOH, AR, Sinopharm), hydrochloric acid (HCl, AR, Sinopharm) were from Sinopharm Reagent Co., Ltd. Tetracycline (TC, $C_{22}H_{24}N_2O_8$, ≥98.0%), chlortetracycline (CTC, $C_{22}H_{23}ClN_2O_8$, ≥95.0%), and oxytetracycline (OTC, $C_{22}H_{25}ClN_2O_9$, ≥99.0%) were purchased from Solarbio (Beijing). Acetonitrile, methanol, and formic acid were chromatographic grades and were purchased from Thermo Fisher Scientific (China) Co., Ltd.

1.2. Characterization

The morphology were characterized by a field emission scanning electron microscope (SEM, JEOL, S-4800). Element distribution information was detected by measuring the energy dispersion X-ray spectrometer (EDS, TN5400, 15 keV). Transmission electron microscope, high-resolution TEM and selective region electron diffraction patterns (TEM, HRTEM, and SAED, JEOL JEM-2100) were used to study the microscopic morphology and structure. The crystal phase structure was measured by powder X-ray diffraction (XRD, Bruker D8, Cu Kα as the source of radiation). The surface compositions and bonding information were obtained by using the X-ray photoelectron energy spectrum and high-resolution spectroscopy (XPS, PHI-5000C ESCA system, with Al K as the radiation source, C $1s$ = 284.6 eV calibration). Optical absorption and photochemical properties were measured by UV-Visible Diffuse spectroscopy (UV-vis DRS), photoluminescence spectroscopy (PL), time-resolved photoluminescence (TRPL) and electrochemical workstations. The UV-Vis spectra of TC were measured using a UV-1800 spectrophotometer (Shimadzu, Japan). Electrochemical impedance spectroscopy (EIS) passed the CHI660B electrochemical

workstation test. Electron spin resonance (ESR) spectra of active free radicals were analyzed on a Bruker A300.

1.3. Catalytic Tests for the degradation of TCs

To verify the photocatalytic degradation performance of $Cu/Cu_2O-Al_2O_3$ on tetracycline antibiotics (including tetracycline (TC), erythromycin (CTC), and oxytomycin (OTC)), the catalytic tests were tested on a multi-tube photocatalytic reaction device (CEL-LAB500, Beijing China Education Orott Co., Ltd.). During the experiments, 15 mg of catalyst was first added to the antibiotic solution (30 mL, 10 mg·L^{-1}). In order to better allow the system to reach adsorption-desorption equilibrium before the reaction and to prevent degradation in the dark, the suspensions were required to stand in the dark for 30 min before turning on the photochemical reactor for the reaction. During degradation, 3 mL of the suspension was removed every 2 min and the catalyst was removed with a 0.22 μm filter membrane. The concentration of TCs in the filtered solution was determined by UV-vis spectrometry. The mineralization efficiency was quantified using a total organic carbon (TOC) analyzer (TOC-VCPH, Shimadzu). The possible intermediates produced during degradation were also analyzed by Liquid Chromatography-Mass Spectrometry (LC-MS, Varian 310)). Moreover, the catalyst after each photocatalytic reaction was centrifuged, washed alternately with ultrapure water and ethanol for multiple times, and then dried for subsequent cyclability and stability test. Verification of the relative strength of the active reactive species in the photocatalytic system was performed with quenching experiments and ESR techniques related to the samples.
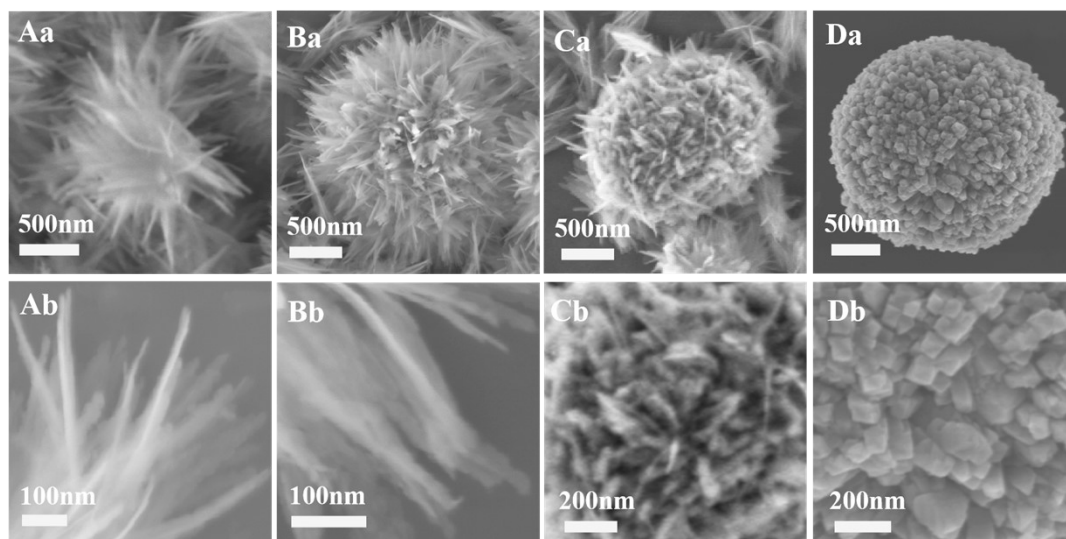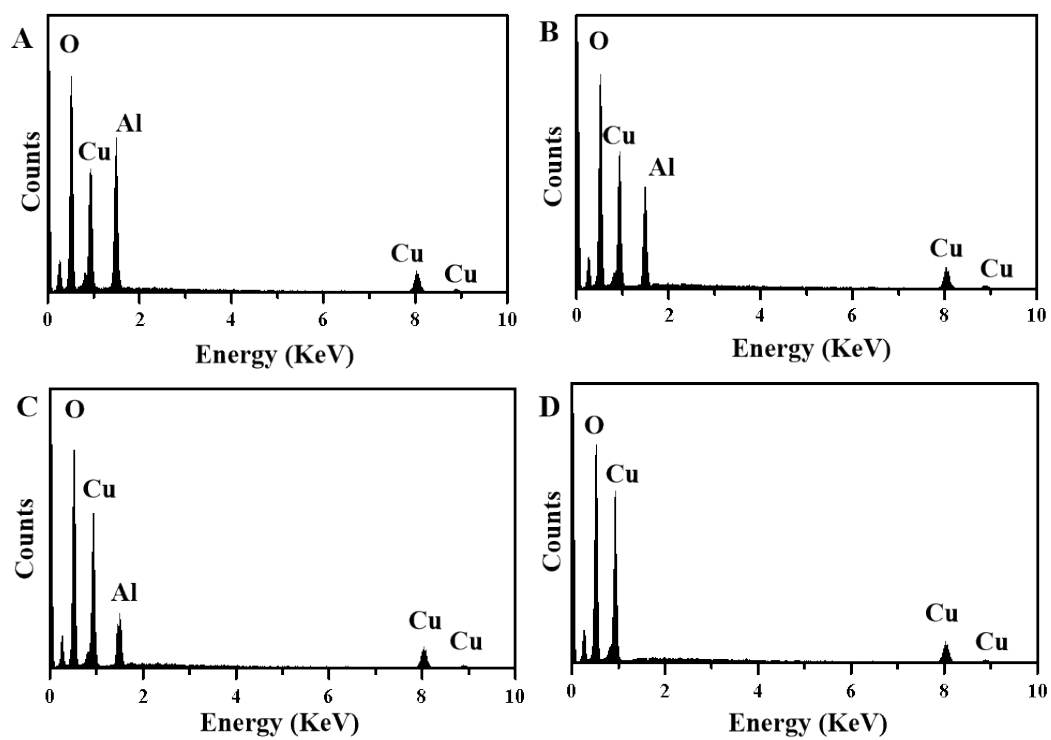
2. Results and Discussion

Fig. S1. SEM images and EDS analysis of 3D CuAl-OH nanostructure with different Cu/Al: (A) 4:6, (B) 6:4, (C) 8:2, (D) 10:0.

Samples	O(%)	Cu(%)	Al(%)
CuAl-OH(A)	54.82	18.07	27.11
CuAl-OH(B)	58.48	24.91	16.61
CuAl-OH(C)	53.49	37.21	9.30
CuAl-OH(D)	57.55	42.45	0.00

Fig. S2. EDS analysis of 3D CuAl-OH nanostructure with different Cu/Al: (A) 4:6, (B) 6:4, (C) 8:2, (D) 10:0.
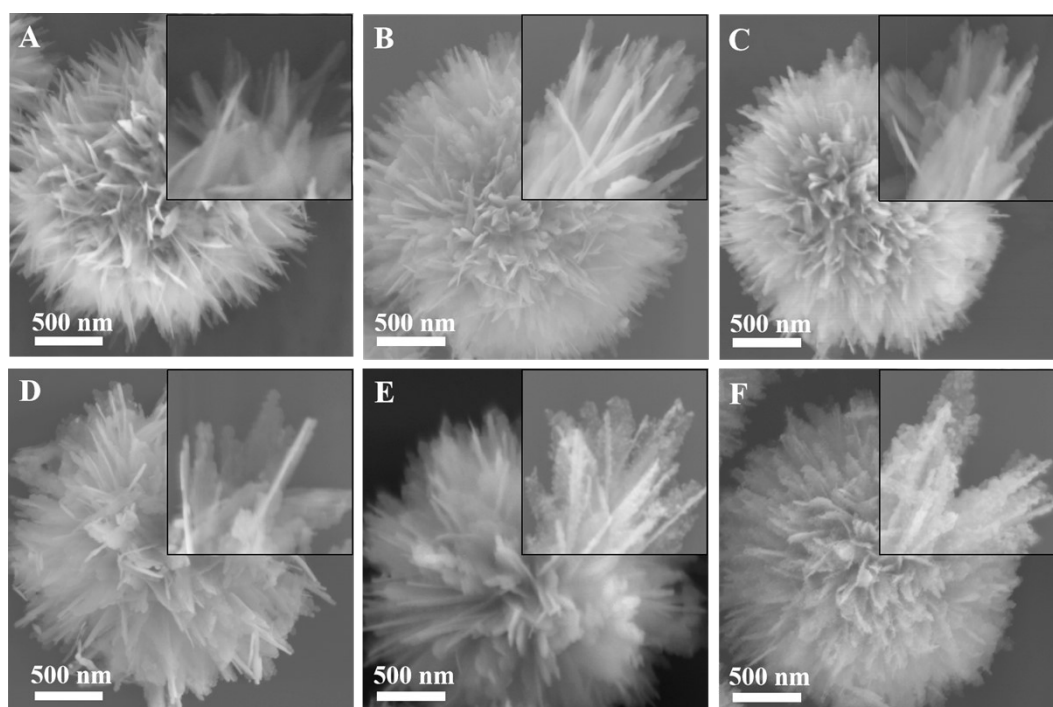
Fig. S3. SEM images of 3D CuAl-OH nanostructure etched by different concentrations of Fe^{3+} ions: (A) 0 mM, (B) 0.5 mM, (C) 1 mM, (D) 1.5 mM, (E) 2 mM, (F) 2.5 mM.
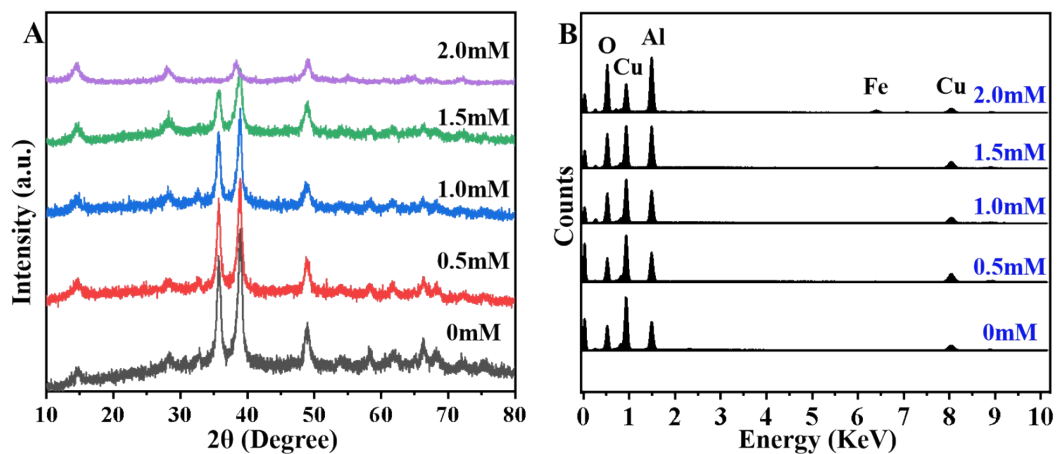
Fig. S4. XRD patterns (A) and EDS analysis (B) of 3D CuAl-OH nanostructure etched by different concentrations of Fe^{3+} ions.
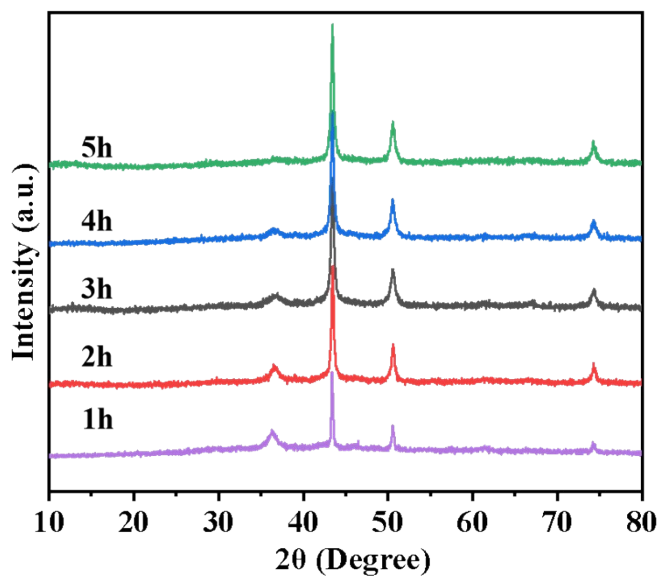
Fig. S5. 3D defect-enriched Cu/Cu_2O-Al_2O_3 ZNR prepared by different reduction time.
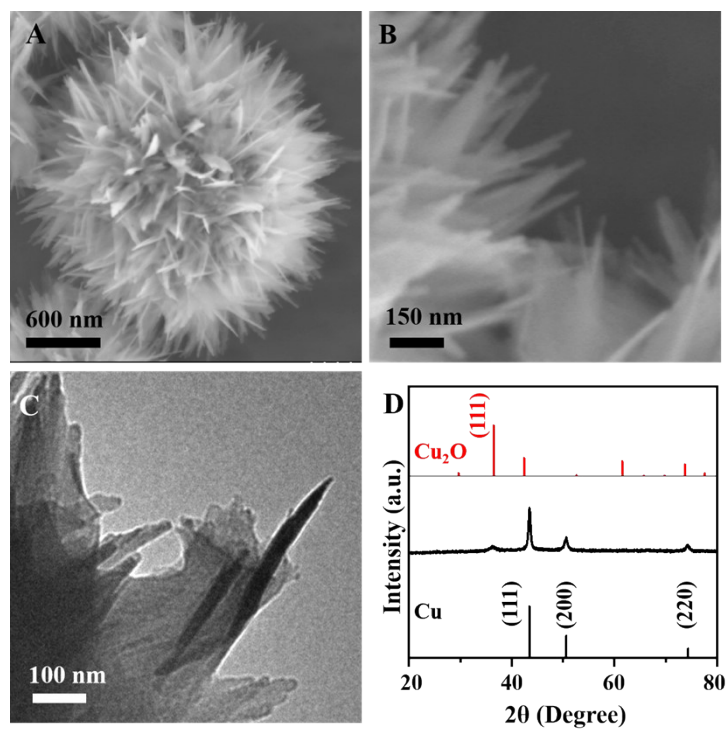
Fig. S6. SEM images (A, B), TEM image (C) and XRD pattern (D) of Cu/Cu$_2$O-Al$_2$O$_3$ NR.
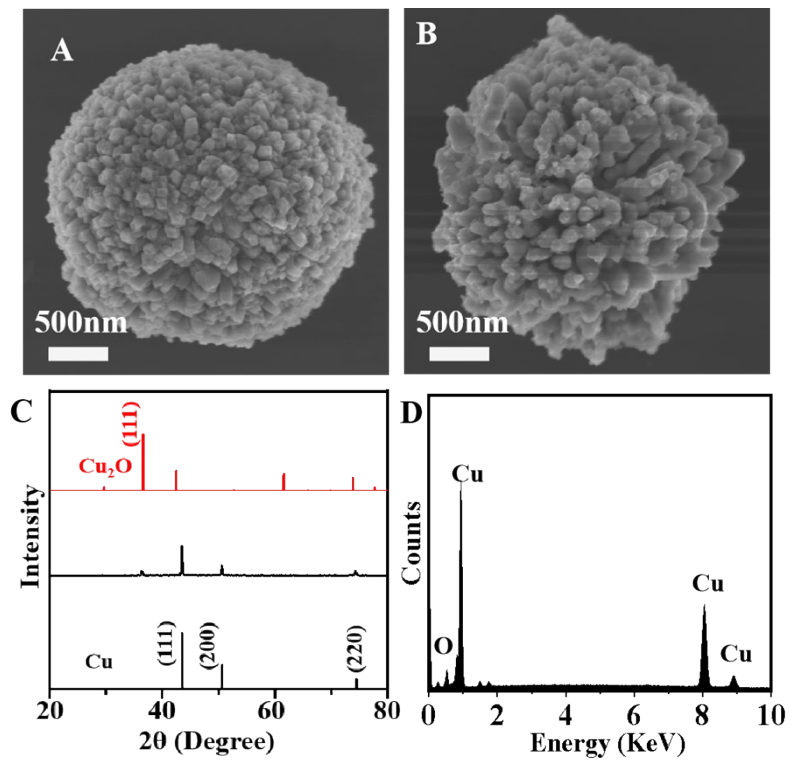
Fig. S7. (A) SEM image of Cu/Cu$_2$O, (B) SEM image, (C) XRD pattern and (D) EDS analysis of Fe-etched Cu/Cu$_2$O nanocomposite.
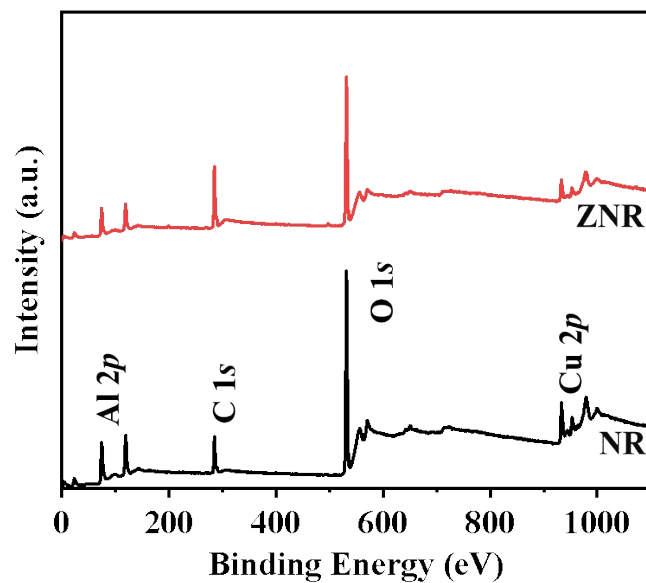
Fig. S8. XPS survey spectrum of Cu/Cu$_2$O-Al$_2$O$_3$ ZNR and Cu/Cu$_2$O-Al$_2$O$_3$ NR.
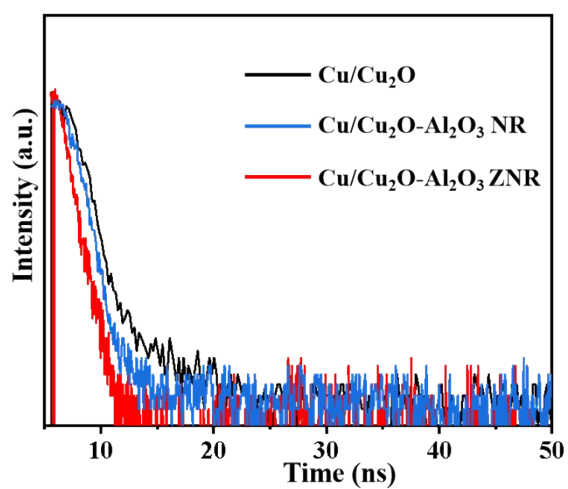
Fig. S9. Time-resolved photo luminescence (TRPL) spectra of Cu/Cu$_2$O-Al$_2$O$_3$ ZNR, Cu/Cu$_2$O-Al$_2$O$_3$ NR and Cu/Cu$_2$O.
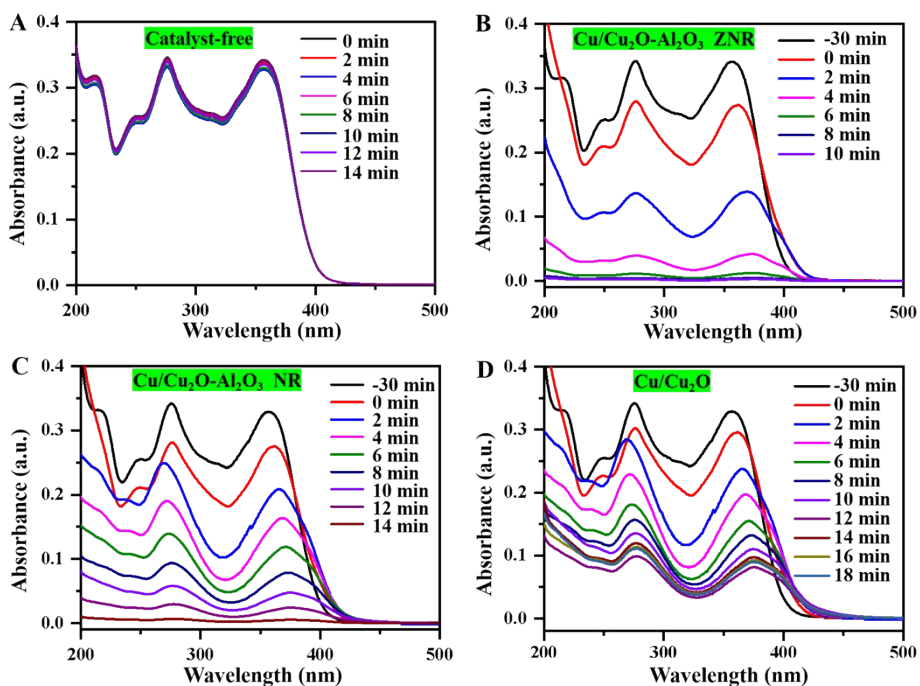
Fig. S10. UV-vis spectra of TC degradation catalyzed by the prepared catalysts under visible-light irradiation: (A) catalyst-free, (B) Cu/Cu$_2$O-Al$_2$O$_3$ ZNR, (C) Cu/Cu$_2$O-Al$_2$O$_3$ NR and (D) Cu/Cu$_2$O.
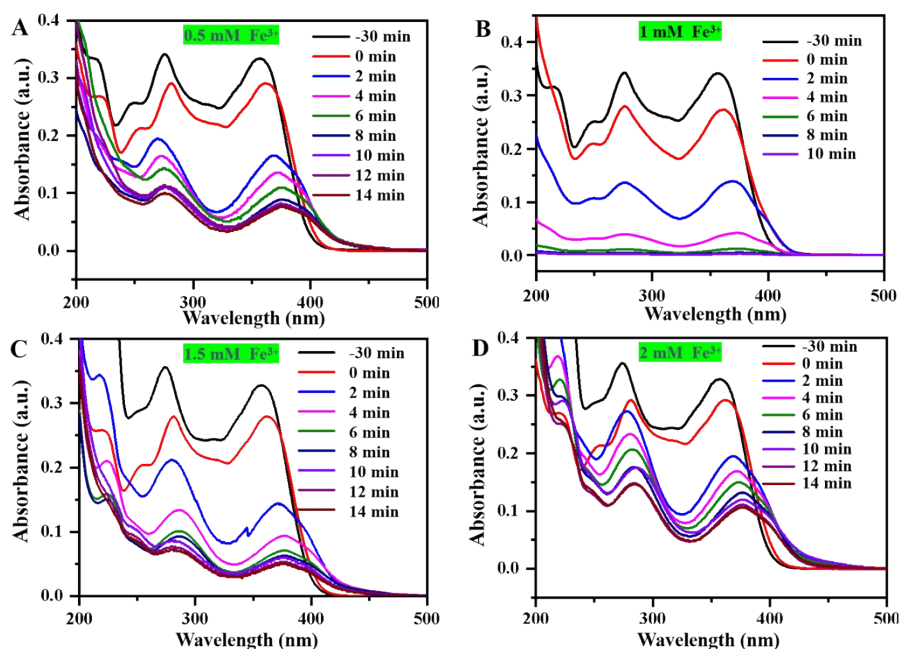
Fig. S11. UV-vis spectra of TC degradation for the catalysts treated with different concentrations of Fe^{3+}: (A) 0.5mM, (B) 1mM, (C) 1.5mM and (D) 2mM.
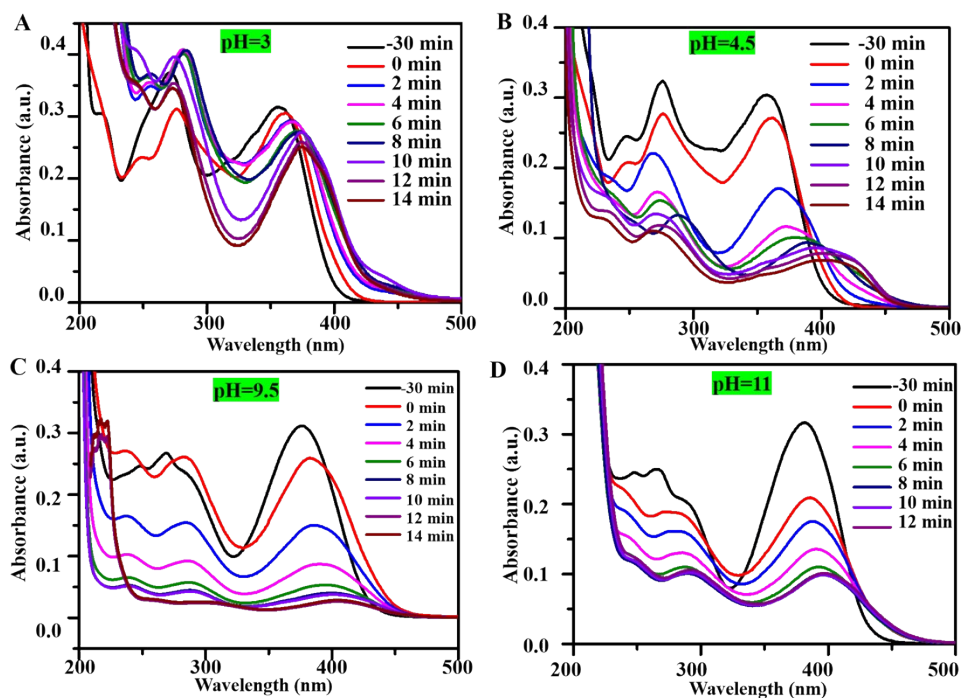
Fig. S12. UV-vis spectra of TC degradation catalyzed by Cu/Cu$_2$O-Al$_2$O$_3$ ZNR with different initial pH : (A) pH=3, (B) pH=4.5, (C) pH=9.5 and (D) pH=11.
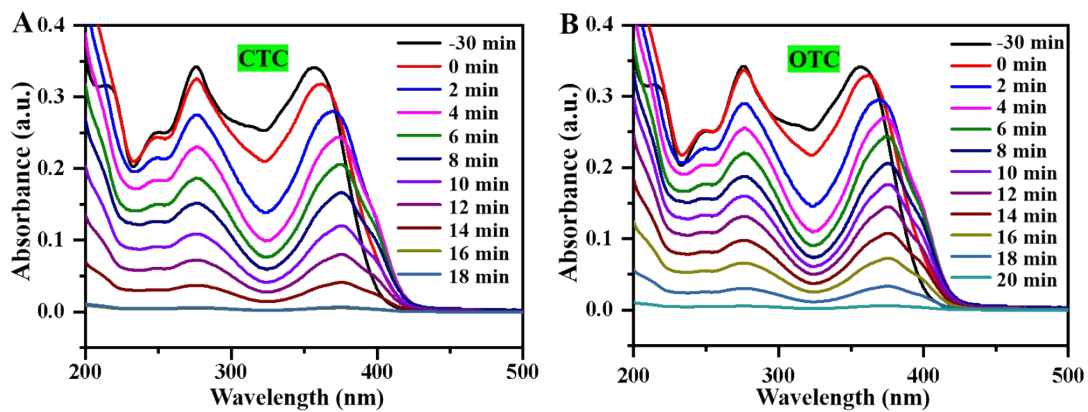
Fig. S13. UV-vis spectra for the degradation of CTC and OTC catalyzed by Cu/Cu$_2$O-Al$_2$O$_3$ ZNR catalyst
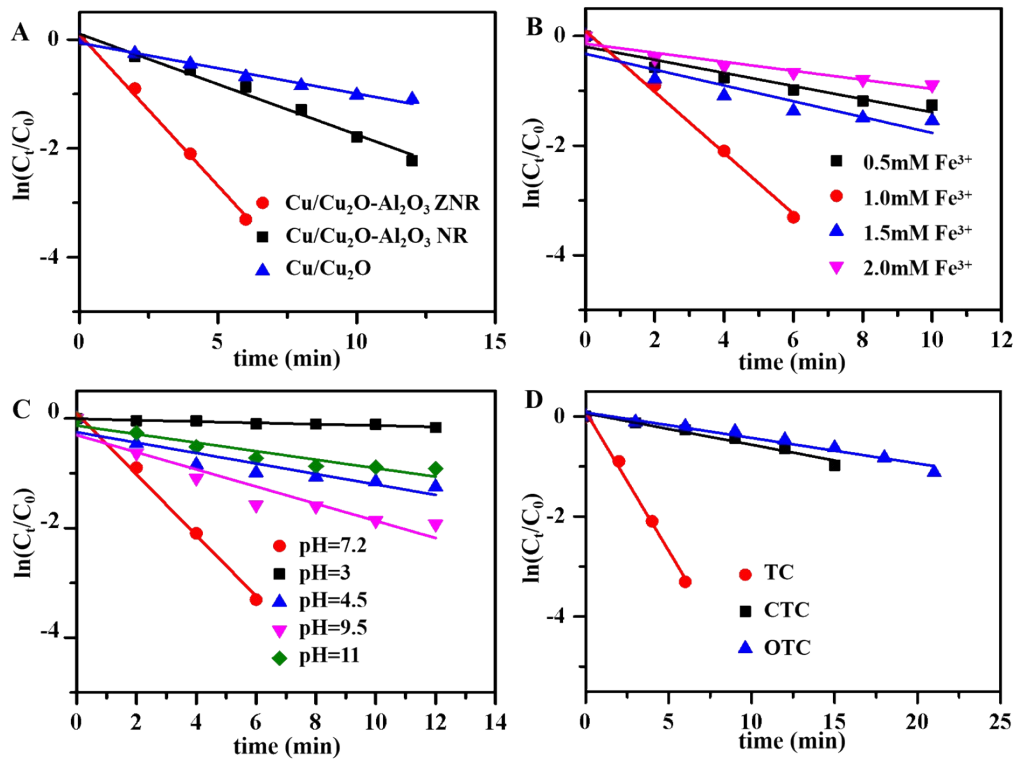
Fig. S14. $\ln C_t/C_0$ versus time for the degradation of TCs in different catalysis system: (A) different catalysts, (B) different etching concentrations of Fe^{3+}, (C) different pH values, (D) different TCs.
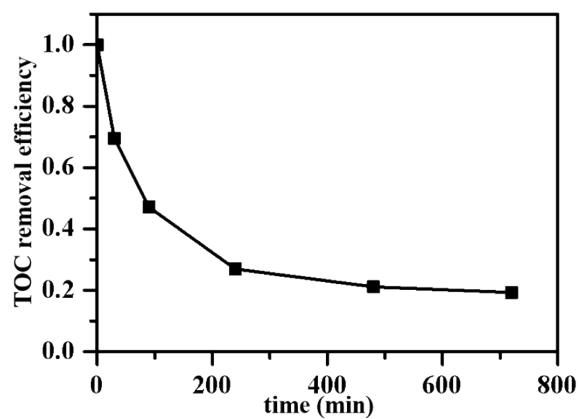
Fig. S15. The TOC removal efficiency using the $Cu/Cu_2O-Al_2O_3$ ZNR catalyst.
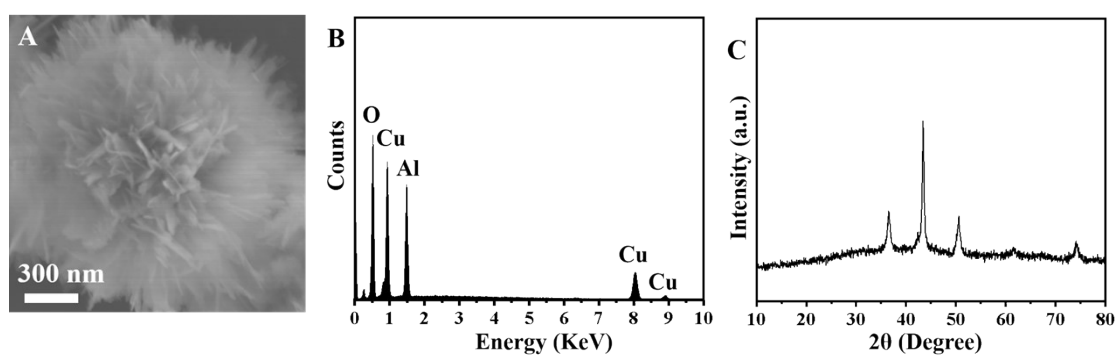
Fig. S16. The SEM image (A), EDS analysis (B) and XRD pattern (C) of Cu/Cu$_2$O-Al$_2$O$_3$ ZNR catalyst after five recycling tests.
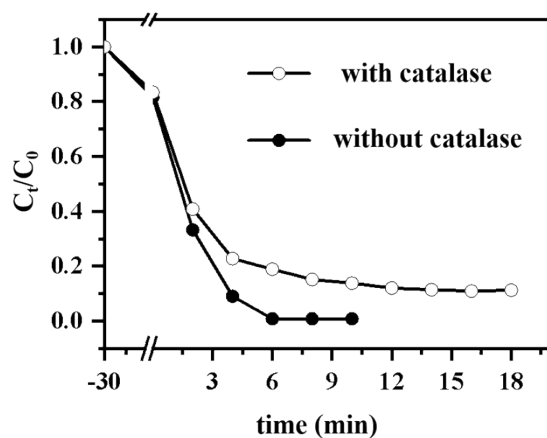
Fig. S17. Profiles of TC degradation catalyzed by Cu/Cu$_2$O-Al$_2$O$_3$ ZNR nanocomposite with catalase (hollow) and without catalase (solid).
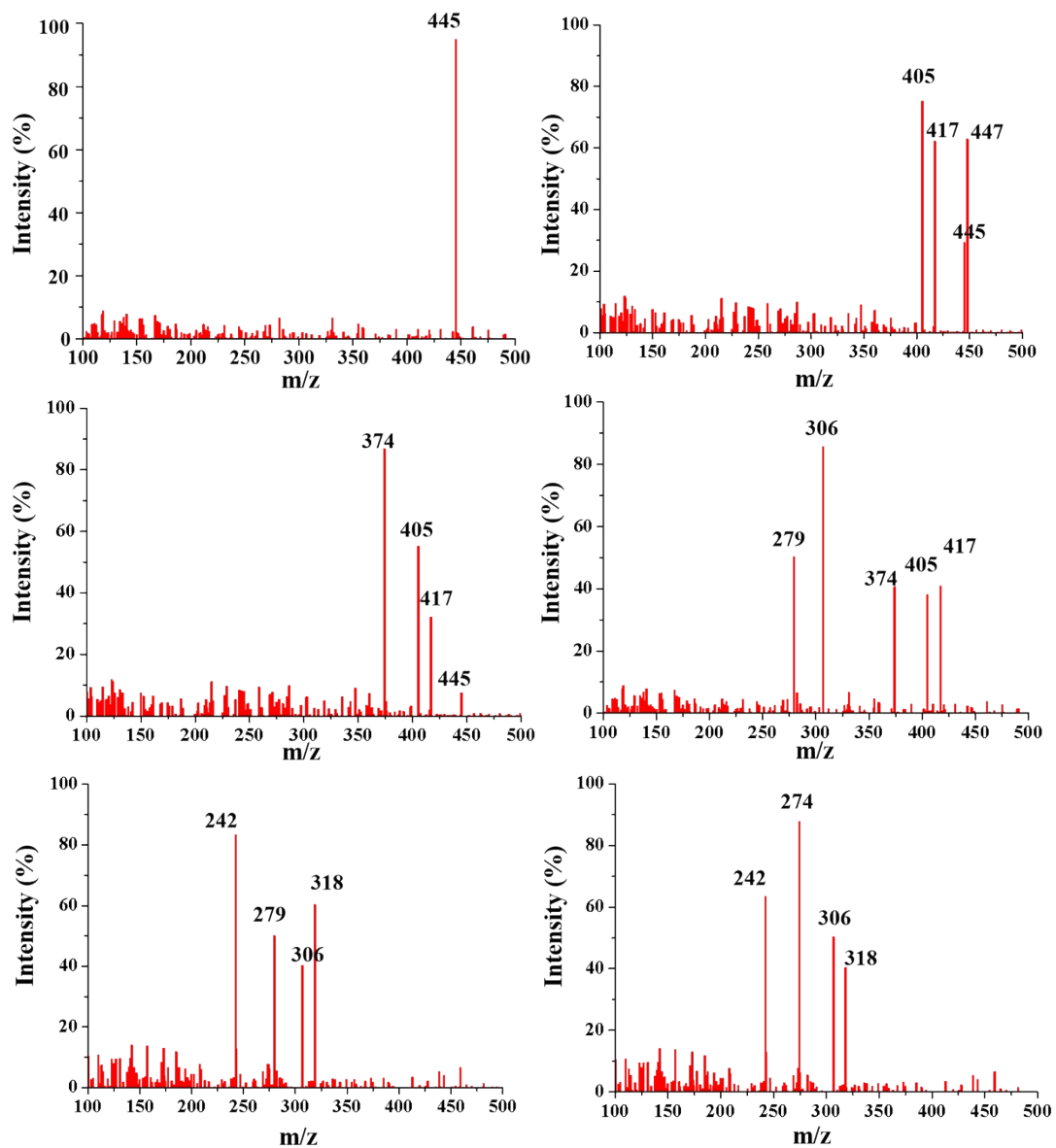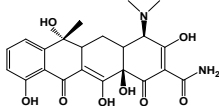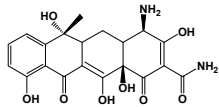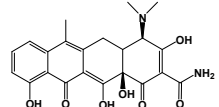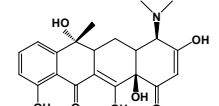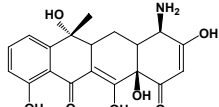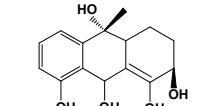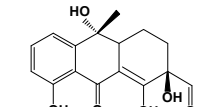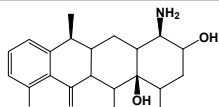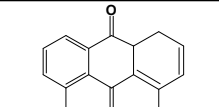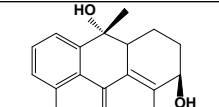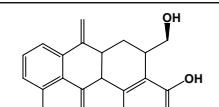
Fig. S18. LC-MS spectra of intermediates in TC degradation for Cu/Cu$_2$O-Al$_2$O$_3$ ZNR catalyst.

Table S1. Potential intermediates detected during TC degradation catalyzed by Cu/Cu$_2$O-Al$_2$O$_3$ ZNR under visible light irradiation.

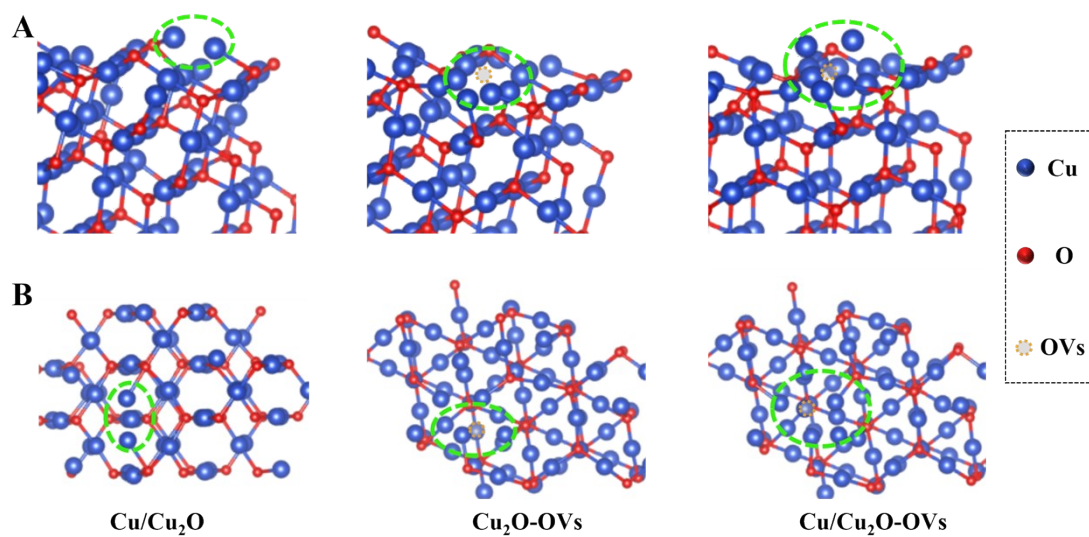| Number	m/z	Molecular formula	Molecular structural formula
TC	445	C$_{22}$H$_{24}$O$_8$N$_2$	
TC1	417	C$_{20}$H$_{21}$O$_8$N$_2$	
TC2	447	C$_{22}$H$_{43}$O$_7$N$_2$	
TC3	405	C$_{21}$H$_{27}$O$_7$N	
TC4	374	C$_{18}$H$_{32}$O$_7$N	
TC5	279	C$_{15}$H$_{19}$O$_5$	
TC6	306	C$_{16}$H$_{18}$O$_6$	
TC7	362	C$_{19}$H$_{24}$O$_6$N	
TC8	242	C$_{14}$H$_{10}$O$_4$	
TC9	274	C$_{15}$H$_{14}$O$_5$	
TC10	318	C$_{17}$H$_{18}$O$_6$	

Fig. S19. The theoretical models Cu/Cu$_2$O, Cu$_2$O-OVs and Cu/Cu$_2$O-OVs: (A) side view, (B) top view.